A Three-Dimensional Fourth-Order Finite-Difference Time-Domain Scheme Using a Symplectic Integrator Propagator

Takuo Hirono, *Member, IEEE*, Wayne Lui, Shunji Seki, *Senior Member, IEEE*, and Yuzo Yoshikuni, *Member, IEEE*

***Abstract*—A new explicit fourth-order finite-difference time-domain (FDTD) scheme for three-dimensional electromagnetic-field simulation is proposed in this paper. A symplectic integrator propagator, which is also known as a decomposition of the exponential operator or a general propagation technique, is directly applied to Maxwell's equations in the scheme. The scheme is nondissipative and saves memory. The Courant stability limit of the scheme is 30% larger than that of the standard FDTD method. The perfectly matched layer absorbing boundary condition is applicable to the scheme. A specific eigenmode of a waveguide is successfully excited in the scheme. Stable and accurate performance is demonstrated by numerical examples.**

***Index Terms*—Electromagnetic fields, FDTD methods, numerical analysis, time-domain analysis.**

I. Introduction

THE finite-difference time-domain (FDTD) method has been used extensively for electromagnetic-field simulation [1], [2]. A problem with this method is its demand for vast computational resources. One solution is to use a scheme whose accuracy is higher than that of the standard FDTD method to reduce the required memory size. Decreasing grid dispersion results in reduced memory usage and CPU time for a given phase accuracy. The standard FDTD method [1] is second-order accurate in time and space. A couple of higher order differencing schemes have been proposed [3]–[8].

One approach to obtaining higher order differencing schemes involves the elimination of the second-order truncation errors in time using the relationship between the third-order differentials in space [3], [4]. When the permittivity or permeability is variable in space, scheme construction by this approach is complicated because of the requirement for the approximations of the second-order space derivatives of the permeability or permittivity. Another approach is the application of the explicit Runge–Kutta method. The schemes using the conventional explicit Runge–Kutta method are dissipative [5]–[7]. Thus, they produce not only phase error, but also amplitude error. Moreover, they require additional memory for temporary storage of data for the internal stages.

Manuscript received February 4, 2000; revised October 16, 2000.

T. Hirono and Y. Yoshikuni are with the NTT Photonics Laboratories, Kanagawa 243-0198, Japan (e-mail: tuhirono@aecl.ntt.co.jp).

W. Lui was with the NTT Photonics Laboratories, Kanagawa 243-0198, Japan. He is now with Lightwave Microsystems, San Jose, CA 95134 USA (e-mail: wlui@lightwavemicro.com).

S. Seki is with Corporate Strategy, NTT Electronics Corporation, Tokyo 150-0043, Japan.

Publisher Item Identifier S 0018-9480(01)07591-3.

The authors proposed a two-dimensional (2-D) scheme with fourth-order accuracy in time and space [8]. The scheme is based on the explicit symplectic integrator, which is a time-integration method specialized for Hamiltonian systems [9], [10]. Schemes using the symplectic integrator are nondissipative and do not require additional memory for temporary data storage. Stable and accurate performance with lower memory usage have been demonstrated [11]. However, the rigorous application of the symplectic integrator to three-dimensional (3-D) problems is rather complicated because it requires discretization of the Hamiltonian of the electromagnetic field in three dimensions. In this paper, the authors directly apply the propagator of the symplectic integrator to Maxwell's equations for the first time and obtain a concise fourth-order scheme. The good performance of the scheme is demonstrated by numerical examples.

II. Formulation

First, we outline the symplectic integrator propagator. The linear differential equation for a vector $\mathbf{x}$ is

$$\frac{d\mathbf{x}}{dt} = C\mathbf{x} \tag{1}$$

where C is a matrix. The solution after a time step Δ_t is expressed by the exponential operator $\exp(\Delta_t C)$ as

$$\mathbf{x}(\Delta_t) = \exp(\Delta_t C)\mathbf{x}(0) \tag{2}$$

$$\exp(\Delta_t C) = I + \Delta_t C + \frac{\Delta_t^2}{2!}C^2 + \frac{\Delta_t^3}{3!}C^3 + \frac{\Delta_t^4}{4!}C^4 + \cdots \tag{3}$$

where $\mathbf{x}(0)$ is the initial value and I is the identity matrix. In general, $\exp(\Delta_t C)$ cannot be obtained explicitly. Here, we further assume that C is the sum of two matrices A and B, whose exponential operators $\exp(\Delta_t A)$ and $\exp(\Delta_t B)$ are easily calculated explicitly. If A and B commute as

$$AB = BA. \tag{4}$$

$\exp(\Delta_t C)$ is easily obtained as

$$\exp(\Delta_t C) = \exp(\Delta_t A)\exp(\Delta_t B). \tag{5}$$

When A and B do not commute, (5) is not valid. In this situation, $\exp(\Delta_t C)$ is approximated by the symplectic integrator propagator. The propagator is the multiproduct of the exponen-

tial operator of A and that of B. The propagator approximates $\exp(\Delta_t C)$ as

$$\exp(\Delta_t C) = \prod_{p=1}^{m} \exp(d_p \Delta_t B) \exp(c_p \Delta_t A) + O\big((\Delta_t)^{n+1}\big) \tag{6}$$

where c_p and d_p are real coefficients characterizing the propagator, n is the order of the approximation, and m is the stage number of the propagator. The propagator has also been referred to as a decomposition of the exponential operator [12] or a general propagation technique [13]. The solution of (1) is approximated by applying the integrator step by step. Coefficients c_p and d_p have been studied extensively for $n < 15$ [12]–[17]. The stage number m is equal to or greater than the order n for the propagators described in the references. Examples of coefficients for second- and fourth-order approximation are listed in Table I. These coefficients obey the symmetry relations $c_p = c_{m+1-p}\,(0 < p < m+1)$, $d_p = d_{m-p}\,(0 < p < m)$, and $d_m = 0$. The second-order coefficients make a propagator equivalent to the so-called leapfrog scheme.

Maxwell's equations in an isotropic, lossless, and sourceless medium are written in a matrix form as

$$\frac{\partial}{\partial t}\begin{pmatrix}\mathbf{H}\\ \mathbf{E}\end{pmatrix} = W\begin{pmatrix}\mathbf{H}\\ \mathbf{E}\end{pmatrix} \tag{7}$$

$$W = \begin{pmatrix}\{0\} & -\mu^{-1}R\\ \varepsilon^{-1}R & \{0\}\end{pmatrix} \tag{8}$$

$$R = \begin{pmatrix} 0 & -\dfrac{\partial}{\partial z} & \dfrac{\partial}{\partial y}\\ \dfrac{\partial}{\partial z} & 0 & -\dfrac{\partial}{\partial x}\\ -\dfrac{\partial}{\partial y} & \dfrac{\partial}{\partial x} & 0\end{pmatrix} \tag{9}$$

where $\mathbf{H}$ is the magnetic-field vector, $\mathbf{E}$ is the electric-field vector, $\{0\}$ is the 3×3 zero matrix, R is the 3×3 matrix representing the curl operator, μ is the permeability, and ε is the permittivity. The evolution of the electromagnetic field during the time-step Δ_t is exactly expressed by the exponential operator $\exp(\Delta_t W)$. The matrix W is the sum of the matrices U and V, i.e.,

$$W = U + V \tag{10}$$

where

$$U = \begin{pmatrix}\{0\} & -\mu^{-1}R\\ \{0\} & \{0\}\end{pmatrix} \tag{11}$$

$$V = \begin{pmatrix}\{0\} & \{0\}\\ \varepsilon^{-1}R & \{0\}\end{pmatrix}. \tag{12}$$

Since U^2 is zero,

$$\exp(\Delta_t U) = I_6 + \Delta_t U \tag{13}$$

where I_6 is the 6×6 identity matrix. The operator $\exp(\Delta_t V)$ is expressed similarly as

$$\exp(\Delta_t V) = I_6 + \Delta_t V. \tag{14}$$

Thus, $\exp(\Delta_t U)$ and $\exp(\Delta_t V)$ are obtained explicitely. The

TABLE I
COEFFICIENTS OF THE SYMPLECTIC INTEGRATOR PROPAGATORS
$(c_p = c_{m+1-p}\ (0 < p < m+1), d_p = d_{m-p}\ (0 < p < m), d_m = 0)$

	2nd-order 2-stage	4th-order 5-stage[a]
c_1	0.5	0.17399689146541
d_1	1.0	0.62337932451322
c_2	0.5	-0.12038504121430
d_2	0.0	-0.12337932451322
c_3	-	0.89277629949778
d_3	-	d_2

[a]Reference 13.

matrices U and V do not cummute, i.e.,

$$UV \neq VU. \tag{15}$$

Therefore, the symplectic integrator is applicable to Maxwell's equations. When one uses coefficients c_p and d_p of order n and substitutes the space difference operators with hth-order accuracy for the first-order partial differential operators in R, an FDTD scheme of nth order in time and hth order in space is obtained. In this paper, the Yee lattice [1], [2] is used for discretizing volume into cells and the space increments in the x-, y-, and z-directions are described as Δ_x, Δ_y, and Δ_z. When the second-order coefficients in Table I and second-order space difference operators, such as

$$\left(\frac{\partial f}{\partial x}\right)_i \approx \frac{f_{i+1/2} - f_{i-1/2}}{\Delta_x} \tag{16}$$

are used, the standard FDTD method is obtained, which is hereafter referred to as the $(2,2)$ scheme. The proposed 3-D fourth-order scheme is obtained, when the fourth-order coefficients in Table I and fourth-order space difference operators, such as

$$\left(\frac{\partial f}{\partial x}\right)_i \approx \frac{27(f_{i+1/2} - f_{i-1/2}) - f_{i+3/2} + f_{i-3/2}}{24\Delta_x} \tag{17}$$

are used. The proposed scheme is referred to as the $(4,4)$ scheme. The time-step diagrams of the $(2,2)$ and $(4,4)$ schemes are shown in Fig. 1. In Fig. 1, thick straight arrows at the top and bottom express the passage of time, and the tick marks on the arrows represent the stages of the schemes. Curved black arrows with the boxes represent the calculations from one stage to the next. The dotted arrows show which electromagnetic component is used in the calculation. In the $(2,2)$ scheme, the calculation of $\exp((1/2)\Delta_t U)$ for the transition from $H^{n-1/2}$ to H^n and the calculation of $\exp((1/2)\Delta_t U)$ for the transition from H^n to $H^{n+1/2}$ are usually combined into one calculation of $\exp(\Delta_t U)$ for the transition from $H^{n-1/2}$ to $H^{n+1/2}$. In the $(4,4)$ scheme, the calculations of $\exp(c_5 \Delta_t U)$ and $\exp(c_1 \Delta_t U)$ can also be combined into one calculation of $\exp((c_5 + c_1)\Delta_t U)$. In this paper, we assume that the permeability is constant throughout the simulation domain. For example, the detailed expressions of the H_z and E_z components at the third stage in the $(4,4)$ scheme are as

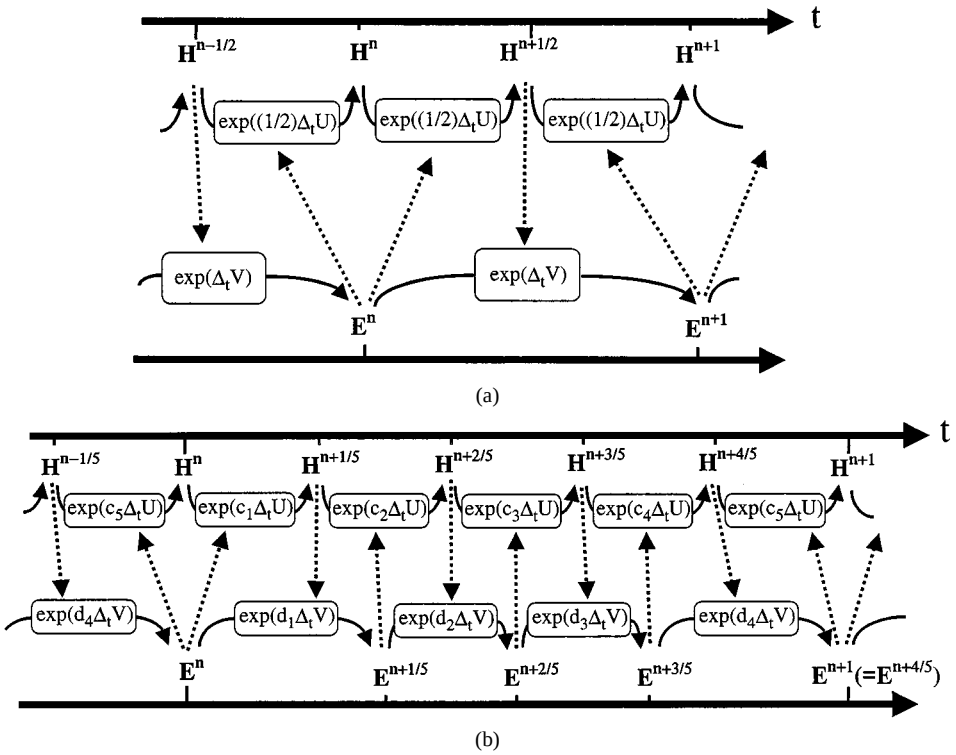

Fig. 1. (a) Time-step diagram of the $(2,2)$ scheme (standard scheme). (b) Time-step diagram of the $(4,4)$ scheme (proposed scheme).

follows:

$$
\begin{aligned}
&H_z^{n+3/5}\left(i+\frac{1}{2},j+\frac{1}{2},k\right)\\
&\quad=H_z^{n+2/5}\left(i+\frac{1}{2},j+\frac{1}{2},k\right)\\
&\qquad-\frac{c_3\Delta_t}{\mu\Delta_x}\left\{\frac{9}{8}\left(E_y^{n+2/5}\left(i+1,j+\frac{1}{2},k\right)\right.\right.\\
&\qquad\qquad\left.-E_y^{n+2/5}\left(i,j+\frac{1}{2},k\right)\right)\\
&\qquad\qquad-\frac{1}{24}\left(E_y^{n+2/5}\left(i+2,j+\frac{1}{2},k\right)\right.\\
&\qquad\qquad\left.\left.-E_y^{n+2/5}\left(i-1,j+\frac{1}{2},k\right)\right)\right\}\\
&\qquad+\frac{c_3\Delta_t}{\mu\Delta_y}\left\{\frac{9}{8}\left(E_x^{n+2/5}\left(i+\frac{1}{2},j+1,k\right)\right.\right.\\
&\qquad\qquad\left.-E_x^{n+2/5}\left(i+\frac{1}{2},j,k\right)\right)\\
&\qquad\qquad-\frac{1}{24}\left(E_x^{n+2/5}\left(i+\frac{1}{2},j+2,k\right)\right.\\
&\qquad\qquad\left.\left.-E_x^{n+2/5}\left(i+\frac{1}{2},j-1,k\right)\right)\right\}
\end{aligned}
\tag{18}
$$

$$
\begin{aligned}
&E_z^{n+3/5}\left(i,j,k+\frac{1}{2}\right)\\
&\quad=E_z^{n+2/5}\left(i,j,k+\frac{1}{2}\right)\\
&\qquad+\frac{d_3\Delta_t}{\Delta_x}\left\{\frac{9}{8\varepsilon_{1,x}\left(i,j,k+\frac{1}{2}\right)}\right.\\
&\qquad\qquad\times\left(H_y^{n+3/5}\left(i+\frac{1}{2},j,k+\frac{1}{2}\right)\right.\\
&\qquad\qquad\left.-H_y^{n+3/5}\left(i-\frac{1}{2},j,k+\frac{1}{2}\right)\right)\\
&\qquad\qquad-\frac{1}{24\varepsilon_{2,x}\left(i,j,k+\frac{1}{2}\right)}\\
&\qquad\qquad\times\left(H_y^{n+3/5}\left(i+\frac{3}{2},j,k+\frac{1}{2}\right)\right.\\
&\qquad\qquad\left.\left.-H_y^{n+3/5}\left(i-\frac{3}{2},j,k+\frac{1}{2}\right)\right)\right\}\\
&\qquad-\frac{d_3\Delta_t}{\Delta_y}\left\{\frac{9}{8\varepsilon_{1,y}\left(i,j,k+\frac{1}{2}\right)}\right.\\
&\qquad\qquad\times\left(H_x^{n+3/5}\left(i,j+\frac{1}{2},k+\frac{1}{2}\right)\right.\\
&\qquad\qquad\left.-H_x^{n+3/5}\left(i,j-\frac{1}{2},k+\frac{1}{2}\right)\right)\\
&\qquad\qquad-\frac{1}{24\varepsilon_{2,y}\left(i,j,k+\frac{1}{2}\right)}\\
&\qquad\qquad\times\left(H_x^{n+3/5}\left(i,j+\frac{3}{2},k+\frac{1}{2}\right)\right.\\
&\qquad\qquad\left.\left.-H_x^{n+3/5}\left(i,j-\frac{3}{2},k+\frac{1}{2}\right)\right)\right\}
\end{aligned}
\tag{19}
$$

where $\varepsilon_{1,x}(i,j,k+1/2)$, $\varepsilon_{2,x}(i,j,k+1/2)$, $\varepsilon_{1,y}(i,j,k+1/2)$, and $\varepsilon_{2,y}(i,j,k+1/2)$ are the permittivities for the simulation. The calculations for (18) and (19) are, respectively, represented by $\exp(c_3\Delta_t U)$ and $\exp(d_3\Delta_t V)$ in the boxes in Fig. 1(b). Equations (18) and (19) show that, in the $(4,4)$ scheme, the changes in the electromagnetic-field values from one stage to the next are calculated with the fourth-order space difference operator. In the $(2,2)$ scheme, the changes are calculated with the second-order space difference operator. Fig. 1(b) and (18) and (19) show the simple iterative character of the $(4,4)$ scheme. Since the field data is successively rewritten by new data, no additional memory for temporary storage of internal stage data is required. The $(4,4)$ scheme is an improved version of the $(2,2)$ scheme for high accuracy.

In this paper, the authors propose two methods for the setting of the permittivities for the simulation. When the spacial variation of the permittivity is continuous, the permittivity at point $(i,j,k+1/2)$ can be used for $\varepsilon_{1,x}(i,j,k+1/2)$, $\varepsilon_{2,x}(i,j,k+1/2)$, $\varepsilon_{1,y}(i,j,k+1/2)$, and $\varepsilon_{2,y}(i,j,k+1/2)$. This method is referred to as method I. For the case of a dielectric interface in the simulated domain, the setting for the nodes in the vicinity of the interface has not been clarified completely. It is now being studied. For the 2-D TM polarization case, with the interface located on the nodes of the magnetic components, method I brings second-order accuracy in the reflectivity and transmissivity. This is proven by the extended discussion of the interface condition for the $(2,2)$ scheme [18]. At present, the authors conjecture that the following method (method II) gives accurate results for an ordinary problem with arbitrarily arranged dielectric interfaces. The averaged permittivity over the segment between $(i+1/2,j,k+1/2)$ and $(i-1/2,j,k+1/2)$ is used for $\varepsilon_{1,x}(i,j,k+1/2)$, the averaged permittivity over the segment between $(i+3/2,j,k+1/2)$ and $(i-3/2,j,k+1/2)$ for $\varepsilon_{2,x}(i,j,k+1/2)$, the averaged permittivity over the segment between $(i,j+1/2,k+1/2)$ and $(i,j-1/2,k+1/2)$ for $\varepsilon_{1,y}(i,j,k+1/2)$, and the averaged permittivity over the segment between $(i,j+3/2,k+1/2)$ and $(i,j-3/2,k+1/2)$ for $\varepsilon_{2,y}(i,j,k+1/2)$.

The above basic formulation can be extended for a medium with loss and/or a source. When the medium has conductivity, matrices U, V, $\exp(\Delta_t U)$, and $\exp(\Delta_t V)$ are modified to (20)–(23), shown at the bottom of this page, where σ^* is the magnetic conductivity, σ is the electric conductivity, and I_3 is the 3×3 identity matrix, and the fourth-order symplectic integrator propagator is still applicable. The fourth-order approximations for exponential functions

$$\exp(-q)\approx\frac{1-\frac{q}{2}+\frac{q^2}{12}}{1+\frac{q}{2}+\frac{q^2}{12}} \tag{24}$$

$$\frac{1-\exp(-q)}{q}\approx\frac{1-\frac{q}{10}+\frac{q^2}{60}}{1+\frac{2q}{5}+\frac{q^2}{60}} \tag{25}$$

are useful for the numerical calculation of $\exp(\Delta_t U_{\rm abs})$ and $\exp(\Delta_t V_{\rm abs})$. This modified scheme is also applicable to perfectly matched layers (PMLs) [19]. The reflectivity of the PML for the $(4,4)$ scheme is as low as that for the $(2,2)$ scheme [20].

When the source exists, the term expressing it is added to the expressions for field evolution. For example, when the z-component of the current density $J_z(x,y,z,t)$ is not zero, the term $s^{n+3/5}(i,j,k+1/2)$, where

$$s^{n+3/5}\left(i,j,k+\frac{1}{2}\right)=-\frac{d_3\Delta_t}{\varepsilon_1\left(i,j,k+\frac{1}{2}\right)}\times J_z\left(i,j,k+\frac{1}{2}\cdot\left(n+\Sigma_{p=1}^{3}c_p\right)\Delta_t\right) \tag{26}$$

is added to the right-hand side of (19).

III. Basic Properties of the Scheme

The features of the scheme are assessed by the solution growth factor α of a numerical wave mode in a grid. The factor

$$U_{\rm abs}=\begin{pmatrix}-\mu^{-1}\sigma^* I_3 & -\mu^{-1}R\\ \{0\} & \{0\}\end{pmatrix} \tag{20}$$

$$V_{\rm abs}=\begin{pmatrix}\{0\} & \{0\}\\ \varepsilon^{-1}R & -\varepsilon^{-1}\sigma I_3\end{pmatrix} \tag{21}$$

$$\exp(\Delta_t U_{\rm abs})=\begin{pmatrix}\exp\left(-\frac{\Delta_t\sigma^*}{\mu}\right)I_3 & -\left\{\left(\frac{1-\exp\left(-\frac{\Delta_t\sigma^*}{\mu}\right)}{\sigma^*}\right)\right\}R\\ \{0\} & I_3\end{pmatrix} \tag{22}$$

$$\exp(\Delta_t V_{\rm abs})=\begin{pmatrix}I_3 & \{0\}\\ \left\{\left(\frac{1-\exp\left(-\frac{\Delta_t\sigma}{\varepsilon}\right)}{\sigma}\right)\right\}R & \exp\left(-\frac{\Delta_t\sigma}{\varepsilon}\right)I_3\end{pmatrix} \tag{23}$$

is the ratio of the field amplitude of the numerical mode at a time to that at the time before the time step Δ_t. To guarantee numerical stability of the simulation, the inequality

$$|\alpha| \leq 1 \tag{27}$$

should be satisfied for all numerical modes. The condition in (27) determines the maximum time-step $\Delta_{t,\max}$ attainable with the given space increments Δ_x, Δ_y, and Δ_z. When the modulus of the factor α is equal to one for all numerical modes under the condition $\Delta_t \leq \Delta_{t,\max}$, the scheme is nondissipative.

When the medium is uniform, the factor α for the $(4,4)$ scheme is given by (28)–(34), shown at the bottom of this page, where k_x, k_y, and k_z are, respectively, the components of the wavenumber of the numerical mode in the x-, y-, and z-directions. Since ζ is a real number, the condition in (27) is equivalent to

$$|\zeta| \leq 1. \tag{35}$$

Moreover, if the condition in (35) is satisfied, the modulus of the factor α is equal to one. Thus, the $(4,4)$ scheme is nondissipative. The radian frequency ω of the numerical mode is expressed as

$$\omega = \frac{\arccos(\zeta)}{\Delta_t}. \tag{36}$$

By employing the numerical search on the condition in (35), $\Delta_{t,\max}$ is obtained. The phase velocity error of the scheme is examined using (36).

The stability of the scheme is assessed by the Courant stability limit $\nu_{\max}$, which is obtained from $\Delta_{t,\max}$ for the cubic grid as

$$\nu_{\max} = v_0 \frac{\Delta_{t,\max}}{\Delta_x}. \tag{37}$$

Table II shows the Courant stability limits of the $(2,2)$ and $(4,4)$ schemes. The limit of the $(4,4)$ scheme is 30% larger than that of the $(2,2)$ scheme. Fig. 2 shows the maximum phase velocity error as a function of the cell numbers per wavelength at the stability limit of each scheme. The fourth-order accuracy of the $(4,4)$ scheme, which is built into it, is shown by the solid line.

TABLE II
COURANT STABILITY LIMITS ($\nu_{\max}$) OF THE $(2,2)$ AND $(4,4)$ SCHEMES

	(2, 2)	(4, 4)
2-D	0.707	0.910
3-D	0.577	0.743

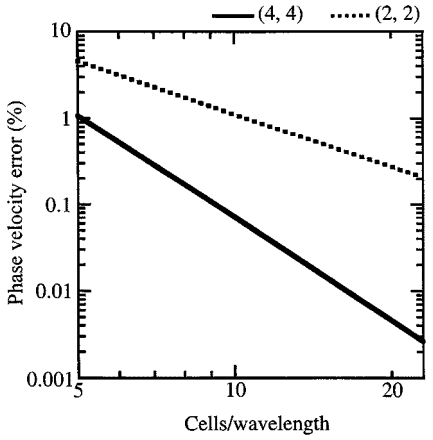

Fig. 2. Phase velocity errors as a function of cell numbers per wavelength on the cubic lattice at the Courant stability limit.

IV. MEMORY AND NUMBER OF COMPUTATIONS

The memory and number of the computations of the $(2,2)$ and $(4,4)$ schemes for 3-D simulation are compared using as the criterion the dispersion error of 1° per wavelength in a cubic lattice. This criterion was proposed in 1993 by Shlager *et al.* [21]. To obtain this accuracy, the required cell number per wavelength N_{cell} is 7.1 for the $(4,4)$ scheme and 19.9 for the $(2,2)$ scheme. On the other hand, the floating point operations per cell

$$\alpha = \zeta \pm \sqrt{\zeta^2 - 1} \tag{28}$$

$$\zeta = 1 + \left(\frac{1}{2}\right) \sum_{p=1}^{m} g_p \Big\{ - v_0^2 \Delta_t^2 \left(\eta_x^2 + \eta_y^2 + \eta_z^2\right) \Big\}^p \tag{29}$$

$$g_p = \sum_{1 \leq i_1 \leq j_1 < i_2 \leq j_2 < \cdots < i_p \leq j_p \leq m} c_{i_1} d_{j_1} c_{i_2} d_{j_2} \cdots c_{i_p} d_{j_p} + \sum_{1 \leq i_1 < j_1 \leq i_2 < j_2 \leq \cdots \leq i_p < j_p \leq m} d_{i_1} c_{j_1} d_{i_2} c_{j_2} \cdots d_{i_p} c_{j_p} \tag{30}$$

$$v_0 = \frac{1}{\sqrt{\varepsilon \mu}} \tag{31}$$

$$\eta_x = j \frac{27\left(e^{-jk_x\Delta_x/2} - e^{jk_x\Delta_x/2}\right) - \left(e^{-3jk_x\Delta_x/2} - e^{3jk_x\Delta_x/2}\right)}{24\Delta_x} \tag{32}$$

$$\eta_y = j \frac{27\left(e^{-jk_y\Delta_y/2} - e^{jk_y\Delta_y/2}\right) - \left(e^{-3jk_y\Delta_y/2} - e^{3jk_y\Delta_y/2}\right)}{24\Delta_y} \tag{33}$$

$$\eta_z = j \frac{27\left(e^{-jk_z\Delta_z/2} - e^{jk_z\Delta_z/2}\right) - \left(e^{-3jk_z\Delta_z/2} - e^{3jk_z\Delta_z/2}\right)}{24\Delta_z} \tag{34}$$

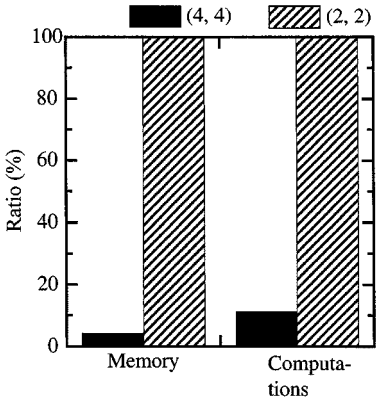

Fig. 3. Comparison of the memory and number of computations in the simulation for cubic cells under the condition of 1°/wavelength dispersion error.

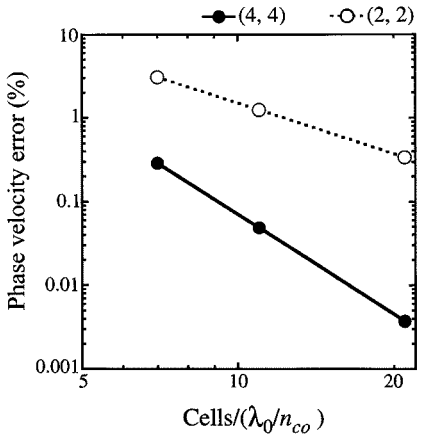

Fig. 4. Phase velocity errors for the HE_{11} mode of the graded-profile fiber.

and time-step $N_{\mathrm{operation}}$ are 240 for the $(4,4)$ scheme and 30 for the $(2,2)$ scheme. The number of computations is evaluated by the product of N_{cell} to the fourth power, $N_{\mathrm{operation}}$, and $\nu_{\max}^{-1}$. The results are shown in Fig. 3. The memory usage for the $(4,4)$ scheme is 4% that for the $(2,2)$ scheme. The number of computations is 10% that the $(2,2)$ scheme.

V. Numerical Examples

A. 3-D Wave Propagation

This example is 3-D wave propagation guided by a graded-profile fiber. The index of refraction $n(r)$ is defined by

$$\begin{aligned} n(r)^2 &= n_{\mathrm{co}}^2, \qquad 0 \le r \le \rho \\ n(r)^2 &= \frac{n_{\mathrm{co}}^2 \rho^2}{r^2}, \quad \rho \le r < \infty \end{aligned} \tag{38}$$

where r is the distance from the fiber axis, n_{co} is the core index, and ρ is the core radius. The HE modes of the fiber were obtained analytically [22]. The propagation of the HE_{11} mode was simulated and the phase velocity was compared to the analytical solution. The n_{co} was 3.0 and ρ was 2.0 μm. The wavelength in a vacuum λ_0 was $1.570796 (= \pi/2)$ μm. We used cubic cells. The fiber axis was set on the line defined by $x = 0$ and $y = 0$. The simulated domain was defined by $(x, y, z) = (\pm 4.0\ \mu\mathrm{m}, \pm 4.0\ \mu\mathrm{m}, \pm \lambda_{\mathrm{fb}}/2)$, where λ_{fb} is the wavelength in the fiber, which is expressed as

$$\lambda_{\mathrm{fb}} = \frac{2\pi}{\beta}, \qquad \beta = 11.9525688\ \mu\mathrm{m} \tag{39}$$

where β is the analytically obtained propagation constant. For the initial condition, analytically obtained values of electromagnetic components were assigned to the nodes in the domain. Since the z-direction length of the domain was equal to the wavelength in the fiber and the magnitude of the field near the boundaries defined by $x = \pm 4.0$ μm or $y = \pm 4.0$ μm was negligibly small, the periodic boundary condition could be applied for the simulation. Method I was used to set the permittivities for the simulation. The Courant–Friedrichs–Levy (CFL) numbers were 0.743 for the $(4,4)$ scheme and 0.577 for the $(2,2)$ scheme. Fig. 4 shows the phase velocity error as a function of the cell numbers per wavelength in the core $(\lambda_0/n_{\mathrm{co}})$. The line for the $(4,4)$ scheme shows its fourth-order accuracy.

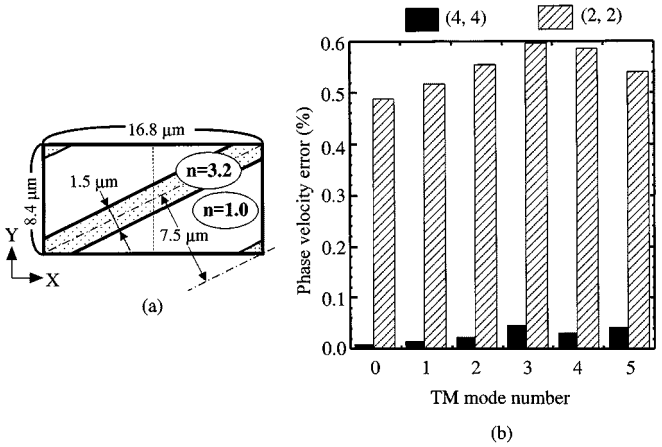

Fig. 5. Phase velocity errors of the TM modes of a 2-D step-profile waveguide. (a) Schematic drawing of the waveguide configuration. (b) Errors for the grid resolution of 15 cells/(wavelength in core region).

B. 2-D Wave Propagation

The propagations of the guided modes along the waveguide with a step index profile were simulated in the 2-D TE polarization case. The phase velocities were compared to the analytical solutions. The refractive indexes of the core and cladding were 3.2 and 1.0, respectively. The core width was 1.5 μm. The wavelength in a vacuum was 1.55 μm. The waveguide supports six guided TM modes. The waveguide configuration is schematically illustrated in Fig. 5(a). A rectangular domain whose sides are along the x- and y-directions was prepared for the simulation. The sides along the x-direction were two times longer than those along the y-direction. The waveguide was set along the diagonal line. The waveguide was inclined to the coordinate axis at an angle of 26.6° $[= \arctan(1/2)]$. The waveguide direction was almost intermediate between the maximum-phase-velocity direction (45°) and the minimum-phase-velocity direction (0°) of the $(2,2)$ scheme. For the initial condition, the analytically obtained values of the electromagnetic components are assigned to the nodes in the domain. The length of the diagonal line was

adjusted to be five times the wavelength in the waveguide $\lambda_{\rm wg}$, which is expressed as

$$\lambda_{\rm wg} = \frac{2\pi}{\beta} \tag{40}$$

where β is the propagation constant of the mode. By this selection of the length of the diagonal line, the assigned field values are periodic at the boundary of the domain. Thus, the periodic boundary condition was used for the simulation. The domain was covered with square cells whose spacing was 1/15 of the free propagation wavelength in the core region. Method II was used to set the permittivities for the simulation. The CFL numbers were 0.743 for the $(4,4)$ scheme and 0.577 for the $(2,2)$ scheme. Fig. 5(b) shows the phase velocity error in the TM modes for the structure. For all guided modes, the error of the $(4,4)$ scheme is less than 1/10 that of the $(2,2)$ scheme. The $(4,4)$ scheme exhibits highly accurate performance in the situation where the refractive index contrast is more than 60%. In order to obtain the same accuracy level as that of the $(4,4)$ scheme with 15 cells/core-wavelength, the $(2,2)$ scheme requires the grid resolution of 60 cells/core-wavelength.

C. Lossy Medium

This example is the simulation of the plane-wave propagation in a medium with the electric conductivity. When ε, μ, and σ are spatially uniform and $\sigma^* = 0$, an analytical calculation shows that a plane wave decays as follows:

$$H_z(x,y,z,t) = \sin(k_x x + k_y y - \omega t)e^{-\tau t} \tag{41}$$

$$E_x(x,y,z,t) = \frac{\mu k_y}{\mathbf{k}^2}\Big\{(-\omega)\sin(k_x x + k_y y - \omega t) + \tau\cos(k_x x + k_y y - \omega t)\Big\}e^{-\tau t} \tag{42}$$

$$E_y(x,y,z,t) = -\frac{\mu k_x}{\mathbf{k}^2}\Big\{(-\omega)\sin(k_x x + k_y y - \omega t) + \tau\cos(k_x x + k_y y - \omega t)\Big\}e^{-\tau t} \tag{43}$$

$$\tau = \frac{\sigma}{2\varepsilon}$$

$$\mathbf{k}^2 = \varepsilon\mu(\omega^2 + \tau^2) \tag{44}$$

where $\mathbf{k} = (k_x, k_y, 0)$ is the wave vector, ω is the angular frequency, and τ is the decay rate. The other field components are zero. In this example, ε, μ, σ, ω, and k_y/k_x were set to ε_0, μ_0, 10^4 S/m, 1213.95/ps, and 1/2. For the initial condition, the field values expressed by (41)–(43) are assigned to the nodes in the rectangular domain similar to that in the previous numerical example. That is, the sides of the domain along the x-direction were two times longer than those along the y-direction and the length of the diagonal line was five times the wavelength. The decay of the wave was simulated using a periodic boundary condition. The cells were square. The CFL numbers were 0.743 for the $(4,4)$ scheme and 0.577 for the $(2,2)$ scheme. Fig. 6 shows the decay rate errors as a function of the cell numbers per wavelength. This figure shows the fourth-order accuracy of the $(4,4)$ scheme for a medium with loss.

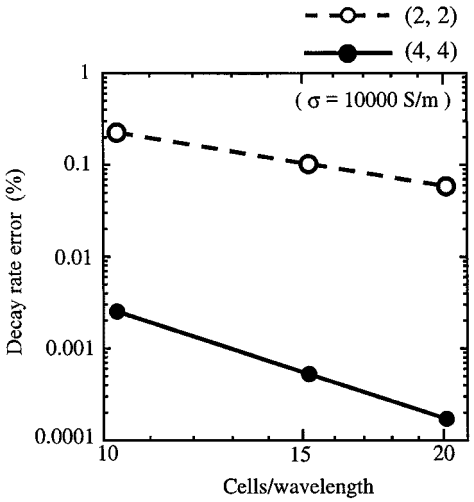

Fig. 6. Decay rate errors as a function of cell numbers per wavelength.

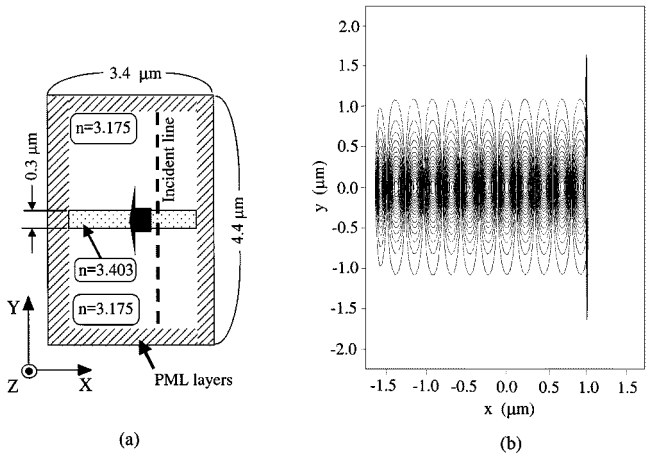

Fig. 7. Unidirectional excitation of the $\rm TM_0$ mode of the 2-D step-profile waveguide. (a) Schematic drawing of the simulated region. (b) Excited H_z distribution.

D. Unidirectional Excitation

This example is the unidirectional excitation of the $\rm TM_0$ mode of a 2-D step-profile waveguide. For the $(2,2)$ scheme, such excitation is outlined in [23]. In the excitation, the transverse components of the excited mode in the vicinity of the incident line are intermittently incorporated with suitable phases in the calculation of each stage. The manner of excitation is extended for the $(4,4)$ scheme. The simulated domain is schematically illustrated in Fig. 7(a). The wavelength in a vacuum was 1.5 μm. The domain with the waveguide was surrounded by 16 PML layers. Fig. 7(b) shows the contour plot of H_z distribution. Δ_x and Δ_y were 0.0125 μm and the CFL number was 0.7. The profiles agree with the analytical ones. The L_2-normed error of the E_x profile is less than 10^{-5}. The example shows the specific waveguide mode can be excited in simulations using the $(4,4)$ scheme.

E. Reflection at a Coated Facet

In this example, waveguide facet reflection was simulated in the 2-D TM polarization case. The waveguide was truncated and the facet was coated with a dielectric layer. A $\rm TE_0$ mode, which was excited by the method described in the previous section, is

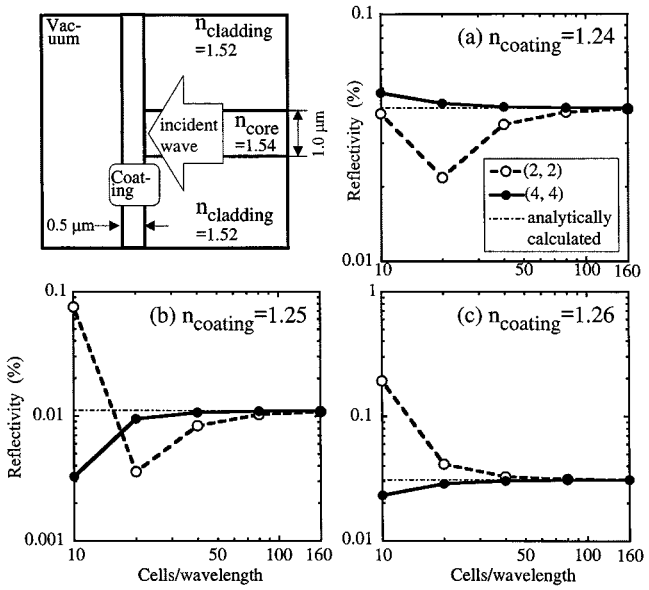

Fig. 8. Simulated reflectivity of the TE_0 mode at the coated facet as a function of the cell number per wavelength in a vacuum, and a schematic drawing of the simulated domain (upper left-hand-side quarter).

incident from the waveguide to the coating. The simulated domain is illustrated in the upper left-hand-side quarter of Fig. 8. The whole domain was surrounded by a 16-cell PML absorber. The effectiveness of the PML absorber in the simulation of reflection at the waveguide facet has been demonstrated in [24]. The wavelength in a vacuum λ_0 was 0.5 μm. The refractive indexes of the coating were 1.24, 1.25, and 1.26. The cells were square and the Δ_x values were 0.05, 0.025, 0.0125, 0.006 25, and 0.003 125 μm in each simulation. The material interfaces were located on the nodes of the magnetic components. Method I was used to set the permittivities for the simulation. The CFL number was 0.7. The reflectivity as a function of the cell numbers per λ_0 is shown in Fig. 8. The analytically calculated reflectivities based on the free-space radiation mode method [25] are also shown by the thin dotted–dashed lines. As the cell number increases, the reflectivity obtained by the $(4, 4)$ scheme converges more rapidly to the analytically calculated reflectivity than that obtained by the $(2, 2)$ scheme.

VI. Summary

A new 3-D explicit fourth-order FDTD scheme has been proposed based on the symplectic integrator propagator. The basic properties of the scheme have been examined theoretically. Several numerical examples have demonstrated its stable and accurate performance. The scheme is expected to be a powerful tool for precise simulation over an extended domain.

Acknowledgment

The authors wish to thank Dr. K. Yokoyama, Noah Consulitng Ltd., Isehara-shi, Kanagawa, Japan, and Dr. K. Kawano, Anritsu Corporation, Atsugi-shi, Kanagawa, Japan, for their encouragement.

References

[1] K. S. Yee, "Numerical solution of initial boundary value problems involving Maxwell's equations in isotropic media," *IEEE Trans. Antennas Propagat.*, vol. AP-14, pp. 302–307, May 1966.

[2] A. Taflove, *Computational Electrodynamics, the Finite-Difference Time-Domain Method*. Norwood, MA: Artech House, 1995.

[3] J. Fang, "Time domain finite difference computation for Maxwell's equations," Ph.D. dissertation, Dept. Elect. Eng., Univ. California at Berkeley, Berkeley, CA, 1989.

[4] T. Deveze, L. Beaulieu, and W. Tabbara, "A fourth order scheme for the FDTD algorithm applied to Maxwell's equations," in *IEEE AP-S Int. Symp. Dig.*, Chicago, IL, 1992, pp. 346–349.

[5] J. L. Young, D. Gaitonde, and J. J. S. Shang, "Toward the construction of a fourth-order difference scheme for transient EM wave simulation: Staggered grid approach," *IEEE Trans. Antennas Propagat.*, vol. 45, pp. 1573–1580, Nov. 1997.

[6] D. W. Zingg, "High-order finite-difference methods in computational electromagnetics," in *IEEE AP-S Int. Symp. Dig.*, Montreal, QC, Canada, 1997, pp. 110–113.

[7] E. Turkel and A. Yefet, "Fourth order method for Maxwell's equations on a staggered mesh," in *IEEE AP-S Int. Symp.*, Montreal, QC, Canada, 1997, pp. 2156–2159.

[8] T. Hirono, W. W. Lui, and K. Yokoyama, "Time-domain simulation of electromagnetic field using a symplectic integrator," *IEEE Microwave Guided Wave Lett.*, vol. 7, pp. 279–281, Sept. 1997.

[9] E. Hairer, S. P. Nørsett, and G. Wanner, *Solving Ordinary Differential Equations I*. Berlin, Germany: Springer-Verlag, 1991, ch. 2.

[10] J. M. Sanz-Serna and M. P. Calvo, *Numerical Hamiltonian Problems*. London, U.K.: Chapman & Hall, 1994.

[11] T. Hirono, W. W. Lui, K. Yokoyama, and S. Seki, "Stability and dispersion of the symplectic fourth-order time-domain schemes for optical field simulation," *J. Lightwave Technol.*, vol. 16, pp. 1915–1920, Oct. 1998.

[12] M. Suzuki, "Fractal decomposition of exponential operators with applications to many-body theories and Monte Carlo simulations," *Phys. Lett. A*, vol. 146, pp. 319–323, June 1990.

[13] B. Hermansson and D. Yevick, "Generalized propagation techniques—Application to semiconductor rib waveguide Y-junctions," *IEEE Photon. Technol. Lett.*, vol. 2, pp. 738–740, Oct. 1990.

[14] H. Yoshida, "Construction of higher order symplectic integrators," *Phys. Lett. A*, vol. 150, pp. 262–268, Nov. 1990.

[15] M. Glasner, D. Yevick, and B. Hermansson, "Sixth-order generalized propagation technique," *Electron. Lett.*, vol. 27, pp. 475–478, Feb. 1991.

[16] E. Forest and R. D. Ruth, "Fourth-order symplectic integration," *Physica D*, vol. 43, pp. 105–117, May 1990.

[17] M. Suzuki, "General nonsymmetric higher-order decomposition of exponential operators and symplectic integrators," *J. Phys. Soc. Jpn.*, vol. 61, pp. 3015–3019, Sept. 1992.

[18] T. Hirono, Y. Shibata, W. W. Lui, S. Seki, and Y. Yoshikuni, "The second-order condition for the dielectric interface orthogonal to the Yee-lattice axis in the FDTD scheme," *IEEE Microwave Guided Wave Lett.*, vol. 10, pp. 359–361, Sept. 2000.

[19] J.-P. Berenger, "A perfectly matched layer for the absorption of electromagnetic waves," *J. Comput. Phys.*, vol. 114, pp. 185–200, Oct. 1994.

[20] T. Hirono, W. W. Lui, and S. Seki, "Successful applications of PML–ABC to the symplectic FDTD scheme with fourth-order accuracy in time and space," in *IEEE MTT-S Int. Microwave Symp. Dig.*, Anaheim, CA, 1999, pp. 1293–1296.

[21] K. L. Shlager, J. G. Moloney, S. L. Ray, and A. F. Peterson, "Relative accuracy of several finite-difference time-domain method in two and three dimensions," *IEEE Trans. Antennas Propagat.*, vol. 41, pp. 1732–1737, Dec. 1993.

[22] A. W. Snyder and J. D. Love, *Optical Waveguide Theory*. London, U.K.: Chapman & Hall, 1995, ch. 12.

[23] S. T. Chu, W. P. Huang, and S. K. Chaudhuri, "Simulation and analysis of waveguide based optical integrated circuits," *Comput. Phys. Commun.*, vol. 68, pp. 451–484, Nov. 1991.

[24] J. Yamauchi, M. Mita, S. Aoki, and H. Nakano, "Analysis of antireflection coatings using the FD-TD method with the PML absorbing boundary condition," *IEEE Photon. Technol. Lett.*, vol. 8, pp. 239–241, Feb. 1996.

[25] P. C. Kendall, D. A. Roberts, P. N. Robson, M. J. Adams, and M. J. Robertson, "New formula for semiconductor laser facet reflectivity," *IEEE Photon. Technol. Lett.*, vol. 5, pp. 148–150, Feb. 1993.

Takuo Hirono (M'98) received the B.S. and M.S. degrees in applied physics and the Ph.D. degree in Material Science from Waseda University, Tokyo, Japan, in 1977,1980, and 1988, respectively.

In 1980, he joined the Electrical Communication Laboratories, NTT, where he was engaged in research on photosensitive materials and bioelectronics. In 1988, he joined the NTT Opto-Electronics Laboratories, where he was active in the device designing, fabrication, and characteristic analysis of semiconductor lasers for optical communications. He has been also active in fabrication of the user interfaces for optical waveguide designing and theoretical analysis of optical waveguides. In 1999, he joined the NTT Photonics Laboratories, Kanagawa, Japan.

Dr. Hirono is a member of the Institute of Electronics, Information and Communication Engineers (IEICE), Japan, the Japan Society of Applied Physics, and the Physical Society of Japan.

Wayne Lui received the B.S. degree from the University of California at Los Angeles (UCLA), in 1981, and the M.S. and Ph.D. degrees from Cornell University, Ithaca, NY, in 1984 and 1991, respectively, all in electrical engineering.

He was with AT&T Bell Laboratories, Allentown, PA, prior to joining the NTT Photonics Laboratories, Kanagawa, Japan, in 1991. Since 2000, he has been with the Lightwave Microsystems Corporation, San Jose, CA, where he designs photonic waveguide devices.

Shunji Seki (M'88–SM'95) received the B.S., M.S., and Ph.D. degrees in applied physics from Waseda University, Tokyo, Japan, in 1979, 1981, and 1990, respectively.

In 1981, he joined the NTT Ibaraki Electrical Communication Laboratories. His early interests included the design and fabrication of polycrystalline silicon devices. From 1987 to 1995, he was involved with numerical modeling and design of photonic devices and circuits at the NTT Photonics Laboratories. From 1991 to 1992, he was a Visiting Scholar at the Beckman Institute for Advanced Science and Technology, University of Illinois at Urbana-Champaign. From 1995 to 2000, he was involved with photonic design automation systems using Internet technology. He is currently a Senior Manager with Corporate Strategy, NTT Electronics Corporation, Tokyo, Japan. His research interests are primarily concerned with computational physics, numerical simulation of photonic devices and circuits, photonic design automation, and high-performance network computing.

Dr. Seki is a member of the Japan Society of Applied Physics, the Institute of Electronics, Information and Communication Engineers (IEICE), Japan, and the IEEE Lasers and Electro-Optics Society (IEEE LEOS) and the IEEE Communications Society (IEEE COMSOC).

Yuzo Yoshikuni (M'94) was born in Tokyo, Japan, in 1954. He received the B.S. M.S., and Ph.D. degrees in applied chemistry from Tokyo University, Tokyo, Japan, in 1977, 1979, and 1983, respectively.

In 1982, he joined the NTT Electrical Communication Laboratory, where he has been engaged in research on single wavelength GaInAsP–InP lasers. His major research has concentrated on device designing and its characteristics analysis, including relevant measurements and computation. He was a Visiting Researcher with the British Telecom Research Laboratories, where he was engaged in the research of semiconductor optical amplifiers. In 1990, he was an Associate Professor with the Research Center for Advanced Science and Technology (RCAST), Tokyo University. He is currently a Senior Research Engineer engaged in research on semiconductor integrated optical devices and tunable lasers at the NTT Photonics Laboratories, Kanagawa, Japan.

Dr. Yoshikuni is a member of the Institute of Electronics, Information and Communication Engineers (IEICE), Japan, the Japan Society of Applied Physics, and the IEEE Lasers and Electro-Optics Society (IEEE LEOS).